PHYSICAL REVIEW B **90**, 180403(R) (2014)

Origin of the charge gap in LaMnPO

D. E. McNally,[1,*] J. W. Simonson,[1] K. W. Post,[2] Z. P. Yin,[3] M. Pezzoli,[1,3] G. J. Smith,[1] V. Leyva,[1] C. Marques,[1] L. DeBeer-Schmitt,[4] A. I. Kolesnikov,[4] Y. Zhao,[5] J. W. Lynn,[5] D. N. Basov,[2] G. Kotliar,[3] and M. C. Aronson[1,6]

[1]*Department of Physics and Astronomy, Stony Brook University, Stony Brook, New York 11794-3800, USA*

[2]*Department of Physics, University of California, San Diego, La Jolla, California 92093-0319, USA*

[3]*Department of Physics and Astronomy, Rutgers University, Piscataway, New Jersey 08854, USA*

[4]*Neutron Scattering Sciences Division, Oak Ridge National Laboratory, Oak Ridge, Tennessee 37831-6473, USA*

[5]*NIST Center for Neutron Research, National Institute of Standards and Technology, Gaithersburg, Maryland 20899, USA*

[6]*Condensed Matter Physics and Materials Science Department, Brookhaven National Laboratory, Upton, New York 11973-5000, USA*

(Received 23 February 2014; revised manuscript received 2 November 2014; published 18 November 2014)

We present high temperature inelastic neutron scattering and magnetic susceptibility measurements of the antiferromagnetic insulator LaMnPO that are consistent with the presence of two-dimensional magnetic correlations up to a temperature $T_{\max} \approx 700$ K $\gg T_N = 375$ K, the Néel temperature. Optical transmission measurements show the $T = 300$ K direct charge gap $\Delta = 1$ eV has decreased only marginally by 500 K and suggest it decreases by only 10% at $T_{\max}$. Density functional theory and dynamical mean-field theory calculations reproduce a direct charge gap in paramagnetic LaMnPO only when a strong Hund's coupling $J_H = 0.9$ eV is included, as well as on-site Hubbard $U = 8$ eV. Our results show that LaMnPO is a Mott-Hund's insulator, in which the charge gap is rather insensitive to antiferromagnetic exchange coupling.

DOI: 10.1103/PhysRevB.90.180403 PACS number(s): 71.30.+h, 74.70.Xa, 75.50.Ee

The metal-insulator transition in correlated electron systems, where electron states transform from itinerant to localized, has long been one of the central themes of condensed matter physics [1]. In a prototypical Mott transition [2], increasing the ratio U/t of the on-site Hubbard U to the kinetic hopping t leads to the enhancement of the effective mass of initially itinerant electrons and to spin fluctuations that can drive magnetic order. When U/t surpasses a critical value, the electrons become spatially localized and a metal-insulator transition (MIT) occurs, driven by the formation of a charge gap. Often, the localized electrons are moment bearing, and magnetic order accompanies the MIT. Thus, electronic localization transitions often involve two different instabilities: magnetic order, involving spontaneous symmetry breaking, and a metal-insulator transition that connects an electronic structure with a nonzero density of states at the Fermi surface to an electronic structure with a charge gap.

Recently, Mn-pnictide compounds have received widespread attention because they are magnetic insulators [3–5] as are the parent compounds of the cuprate high temperature superconductors (HTSCs) [6] while adopting the same crystal structures as the metallic parent compounds of the Fe-based HTSC [7,8]. Suppressing the magnetic order and driving an insulating Mn-pnictide across a MIT could lead to a more correlated version of their Fe-based counterparts, where even higher temperature superconductivity may be observed [5,9,10]. However, superconductivity has yet to be observed in a Mn-based compound. Unlike the cuprates, the multiorbital character of the Fe and Mn-pnictides calls for a full description of the MIT that includes not only the Hubbard U, but also the Hund's interaction J_H and possibly Heisenberg exchange interaction J. In these systems, antiferromagnetic (AF) correlations can stabilize an insulating state when the spin flip energy $\propto J$ is comparable to the charge gap Δ [11]. In addition, long range AF order alone can stabilize a gap in a Slater insulator, which would then vanish at T_N [12]. The importance of these interactions has been established in the metallic Fe-pnictides [13], but so far their impact on the isostructural and insulating Mn compounds is not well understood.

Previous measurements show that LaMnPO can be driven through a MIT using pressure but not doping. Ambient pressure LaMnPO is an insulator with $\Delta = 1$ eV [14]. Checkerboard AF order is found below the Néel temperature $T_N = 375$ K with a $T \to 0$ K ordered moment of $3.2\mu_B$/Mn, much reduced from the high spin value of $5\mu_B$/Mn predicted by Hund's rules. The low value of the ordered moment, coupled with significant valence fluctuations detected in x-ray absorption measurements and also in density functional theory plus dynamical mean-field theory (DFT + DMFT) calculations, suggests that ambient pressure LaMnPO is near a MIT [5]. However, doping 28% fluorine into LaMnPO had a minimal effect on the charge gap and ordered moment and no other suitable dopant has been identified [14]. In contrast, pressure drives a MIT in LaMnPO at 20 GPa, followed by AF order collapse at ≈30 GPa [15]. This separation of charge and magnetic instabilities in pressurized LaMnPO adds new urgency to uncovering the origin of the charge gap and its relationship to magnetic order.

We present here experimental and theoretical evidence that together clarifies the relative importance of the Hubbard U, Hund's J_H, and Heisenberg J for stabilizing the charge gap Δ in LaMnPO. Our inelastic neutron scattering (INS) measurements determine the nearest and next-nearest exchange interactions $J_{1,2}$, which are much smaller than Δ. LaMnPO is found to be a quasi-two-dimensional (2D) AF with magnetic correlations persisting to ≈700 K, far above $T_N = 375$ K. Optical measurements indicate that Δ has decreased by only 10% at ≈700 K, where magnetic correlations have vanished, compared to its value deep in the AF phase $T \ll T_N$. This is

*daniel.mcnally@stonybrook.edu

evidence that $J_{1,2}$ play only a minimal role in setting the size of Δ in LaMnPO. DFT + DMFT calculations show instead that a large J_H as well as U are required to reproduce the charge gap observed in both the AF and paramagnetic (PM) states. The Mn-pnictide LaMnPO is thus a Mott-Hund's insulator, analogous to the Hund's metal from which superconductivity emerges in the Fe-pnictides.

INS at $T > T_N = 375$ K was carried out with a fixed final energy of 14.7 meV on the BT-7 triple axis spectrometer at the NIST Center for Neutron Research on 13 g of powder prepared by a solid state reaction [16,17]. INS at $T = 5$ K was performed with an incident energy of 250 meV, with the Fermi 2 chopper set to 600 Hz and the T0 chopper set to 120 Hz, at the SEQUIOA time of flight spectrometer at the Spallation Neutron Source at Oak Ridge National Laboratory [18]. Infrared transmission measurements were carried out on single crystals of LaMnPO grown from NaCl-KCl flux [14] using a Bruker Vertex v/70 Fourier transform infrared (FT-IR) spectrometer coupled to a high temperature sample stage. Magnetic susceptibility measurements were performed from 1.8 to 300 K on a collection of single crystals coaligned along the c axis using a Quantum Design magnetic property measurement system and from 300 to 1000 K on a powder sample using the vibrating sample magnetometer option of a Quantum Design physical property measurement system.

The electronic structure of LaMnPO was determined using DFT + DMFT [19,20] which is based on the full-potential linear augmented plane wave method implemented in WIEN2K [21], with the generalized gradient approximation to the exchange-correlation functional [22]. We use the experimentally determined crystal structure [23]. The convergence of the calculations with respect to number of k points, charge density, total energy, Fermi level, and self-energy reached a similar level to previous publications [5,13].

INS provides a detailed picture of the development of the AF correlations above T_N. Figure 1(a) presents the wave-vector q dependence of the scattered neutron intensity $S(q)$ for $T > T_N = 375$ K and energy transfer $E = 5$ meV. $S(q)$ exhibits two overlapping peaks centered at the AF ordering wave vectors $q_{100} \approx 1.6$ Å^{-1} and $q_{101} \approx 1.75$ Å^{-1}, and we ascribe this enhanced scattering to AF spin correlations. We fit $S(q)$ with the sum of two Lorentzian functions $\sum_{i=1}^{2} \frac{A_i}{(q-q_i)^2+\Gamma^2}$ and a linear background, convoluted with the instrumental resolution function that was always narrower than the observed scattering [24]. Here, i indexes the $q_{100,101}$ peaks, Γ is the width of the peaks, and A_i is a constant. The spin correlation length $\xi = 1/a\Gamma$, in units of the lattice parameter $a = 4.054$ Å, decreases with increasing temperature for energy transfers $E = 5$, 10, and 15 meV and $\xi \to a$ at $T_{\max} \approx 700$ K [inset of Fig. 1(a)]. The onset of a Curie-Weiss susceptibility $\chi \propto 1/T$ is also observed when the short range AF correlations vanish [Fig. 1(b)]. The measured $\chi(T)$ is as expected for a quasi-2D Heisenberg AF, where for $T_N < T < T_{\max}$ short ranged correlations within the Mn planes are present, while only above $T_{\max}$ are the magnetic moments independent [25–27]. Further, $\chi(T)$ is featureless at T_N and almost temperature independent up to 700 K, setting the approximate scale for the dominant exchange interaction J_1 between Mn moments.

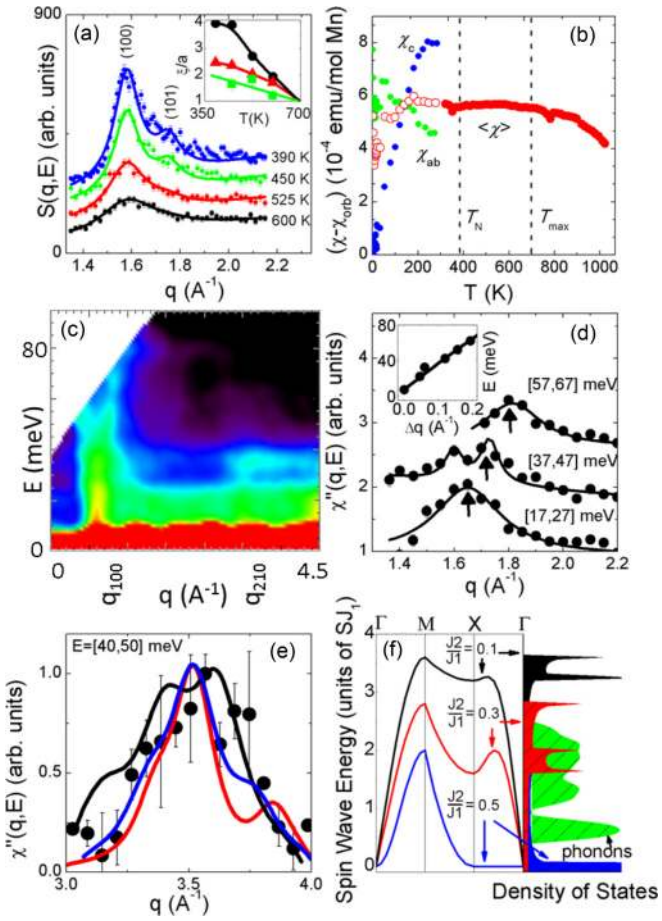

FIG. 1. (Color online) (a) Wave-vector q dependence of the scattered neutron intensity $S(\mathbf{q},E)$ for constant energy transfer $E = 5$ meV at indicated temperatures T. Solid lines are fits as described in the main text. Inset: T dependence of the spatial correlation length ξ in units of the lattice constant a, for $E = 5$ meV (●), 10 meV (red ▲), and 15 meV (green ■). (b) Magnetic susceptibility $\langle\chi\rangle$ of a collection of single crystals (red ○) $\langle\chi\rangle = 2/3(\chi_{ab}) + 1/3(\chi_c)$, where χ_{ab} (green ●) and χ_c (blue ●) were measured with a 1 T field applied in the ab plane and c plane, respectively. The magnetic susceptibility at high temperatures was measured on a powder sample (red ●). Orbital susceptibility $\chi_{\rm orb} = 1.7 \times 10^{-4}$ mu/mol Mn is subtracted from all data. Dashed lines indicate the Néel temperature T_N and mean-field ordering temperature $T_{\max}$. (c) The dynamic susceptibility $\chi''(q,E) = S(q,E)[1 - \exp(-E/k_BT)]$ measured at 5 K. (d) E cuts near the (100) AF zone center summed over the indicated ranges. Solid lines are fits to the sum of two Lorentzians. Inset: Δq, measured relative to q_{100}, for different E. The solid line is a theoretical expression for $\epsilon(q)$ in the Γ-X direction, with $SJ_1 = 34$ meV. Error bars are smaller than points. (e) E cut near (210) averaged on the interval 40–50 meV. The solid lines are the resolution-convoluted intensities expected from a powder-averaged Heisenberg model for $SJ_1 = 18$ meV (black), 34 meV (blue), 48 meV (red). (f) Left: Calculations of $\epsilon(q)$ along different directions in reciprocal space for indicated values of J_2/J_1. Right: Comparison of the experimental density of states (DOS) (green shaded area) to the powder average of $\epsilon(q)$ for values of J_2/J_1 indicated. The low energy part of the DOS is attributed to phonons.

J_1 is determined from the dispersion of the spin waves observed in INS measurements of LaMnPO at $T = 5$ K that

are presented in a contour plot of the dynamic susceptibility $\chi''(q,E)$ [Fig. 1(c)] which has also been corrected for the magnetic form factor of Mn [28]. The most prominent features of the magnetic scattering are the intense dispersive arches centered near $q_{100} = 1.6$ Å^{-1} and $q_{210} = 3.5$ Å^{-1}. These arches merge near $(q,E) = (3$ Å^{-1},80 meV) to complete the spin wave dispersion. E cuts presented in Fig. 1(d) allow us to determine J_1. Here we observe that q_{100} is flanked by two peaks at $q_{100} \pm \Delta q$, which we fit with Lorentzian functions to determine the spin wave dispersion $E(\Delta q)$, plotted in the inset. The spin wave dispersion predicted from the Heisenberg model of a checkerboard AF lattice is $\epsilon(\mathbf{q}) = 4SJ_1\sqrt{1-\cos^2(q_x\frac{a}{2})\cos^2(q_y\frac{a}{2})}$ [29], where S is the total spin and q_x, q_y are the components of $\mathbf{q}$ in the ab plane. Comparing the observed dispersion to this model, we restrict our fits to energies greater than 7 meV in order to accommodate the opening of a spin gap below T_N. The model accounts for the observed dispersion when $SJ_1 = 34 \pm 4$ meV [inset of Fig. 1(d)]. Since our sample is polycrystalline, $\chi''(q,E)$ may include significant contributions from spin waves that originate in different magnetic zones. Figure 1(e) compares $\chi''(q,E)$ near the $q_{210} = 3.5$ Å^{-1} AF zone center to the powder averages of the theoretical dispersions for different values of SJ_1. The experimental data are also consistent with the Heisenberg model for the same value of $SJ_1 = 34$ meV.

Analysis of the total spin wave density of states (SWDOS) shows that a full description by the Heisenberg model requires the inclusion of a second neighbor interaction J_2. Theoretical spin wave dispersions along high symmetry directions in reciprocal space are presented in Fig. 1(f) for values of J_2/J_1 ranging from 0.1 to 0.5. The corresponding powder averaged SWDOS is compared to the observed DOS [Fig. 1(f)] and most resembles the experimental results when $0.2 < J_2/J_1 < 0.4$, yielding SJ_2 in the range 7–14 meV [29]. With these values of exchange interactions, a mean-field ordering temperature $T_{\mathrm{MFT}} = 4(J_1 - J_2)S(S+1)/(3k_B) \geqslant 760$ K is expected [30], similar to the value of $T_{\max}$ determined above.

Our analysis of the INS and magnetization data reveals that $J_{1,2} \ll \Delta$. The ratio of the spin flip energy cost to the gap, $2S^2J/\Delta \approx 0.1$, implies a ≈10% reduction of Δ would occur by $T = 700$ K, where short range AF correlations are no longer present. On the other hand, if $\Delta \to 0$ at T_N, it would identify LaMnPO as a Slater insulator. Both questions can be addressed by measuring the temperature dependence of Δ, using optical transmission measurements $T(\omega)$ through a single crystal of LaMnPO for temperatures up to 500 K. $T(\omega)$ is shown in the inset to Fig. 2(a) at $T = 295$ and 500 K. With increasing ω, a rapid decrease of $T(\omega)$ is observed, consistent with the onset of absorption due to optical excitations across the energy gap Δ. Figure 2(a) presents $[\log(T)/\omega]^2$ for temperatures from 295 to 500 K, where Δ is extracted from linear fits [31]. Δ decreases approximately linearly with increasing temperature [Fig. 2(b)], by ≈5% between 300 and 500 K. Extrapolating these data projects a 10% reduction in Δ by 700 K, where $\xi \to a$, just as predicted above. In addition, $\Delta(T)$ is featureless at T_N, showing that LaMnPO is not a Slater insulator. Given that the exchange interaction plays a small role in gap formation, we turn to electronic structure calculations to explain the origin of the gap.

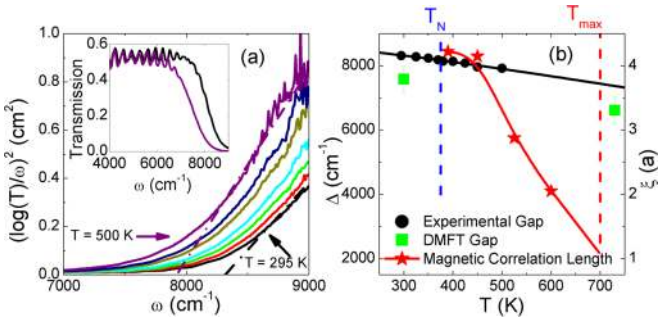

FIG. 2. (Color online) (a) [log(transmission)/wave number]^2 at $T = 295$ K (black), 325 K (red), 350 K (green), 380 K (cyan), 425 K (brown), 450 K (navy blue), 500 K (purple). Dashed lines are fits to the 295 and 500 K data as described in the text. Inset: Transmission data for 295 K (black) and 500 K (purple). (b) The temperature dependence of the experimental direct gap Δ (●), Δ in the AF and PM states determined from DFT + DMFT calculations (green ■), and the experimental AF correlation length ξ.

The importance of correlations for the charge gap in LaMnPO in the AF state have been previously emphasized [5]. Here, we present DFT + DMFT calculations of the electronic structure of LaMnPO that show Hund's coupling J_H plays a decisive role for the formation of a charge gap in the PM state, even when long range magnetic order is no longer present. We begin by presenting in Fig. 3(a) the calculated electronic structure along high symmetry directions in the PM state, using an unreasonably large Hubbard $U = 10$ eV [32–34]. Here, LaMnPO is found to be a metal as there are bands crossing the Fermi level, in direct contradiction to the measured gap $\Delta = 1$ eV.

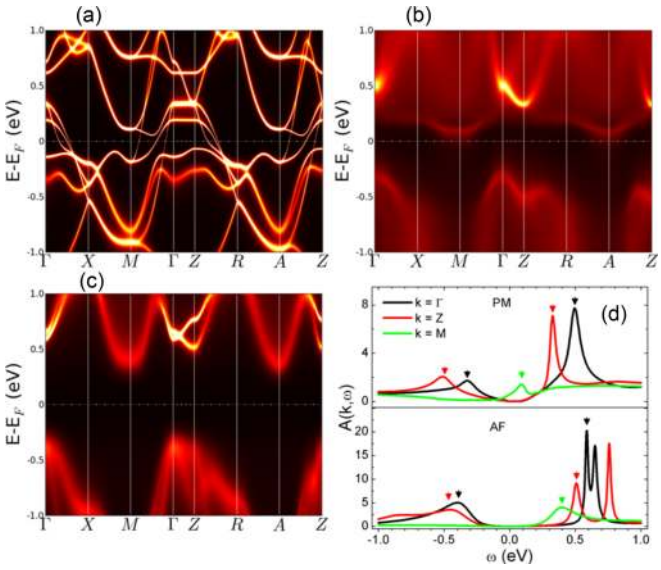

FIG. 3. (Color online) Density functional theory + dynamical mean-field theory (DFT + DMFT) calculations of the band structure of LaMnPO . (a) Paramagnetic (PM) state with Hubbard $U = 10$ eV and Hund's $J_H = 0$ eV. (b) PM state with $U = 8$ eV and $J_H = 0.9$ eV. (c) Antiferromagnetic (AF) state with $U = 8$ eV and $J_H = 0.9$ eV. (d) Spectral function $A(k,\omega)$ at high symmetry points for the calculations shown in (b) and (c). Triangles indicate the peak position of $A(k,\omega)$.

Thus, we can conclude that U is not solely responsible for the charge gap, and LaMnPO cannot be considered a conventional Mott-Hubbard insulator.

Recently, it has been established that J_H is important for the correlations in multiorbital transition metal systems such as the Fe-pnictides [13,34–37]. The first of Hund's empirical rules is that energy is minimized for a maximum spin S on an isolated atom. For Mn^{2+} ions Hund's rule fills all five $3d$ orbitals with parallel spins to maximize S. This results in a significant energy cost in hopping between atoms as any doubly occupied orbitals would reduce S. Consequently, it has been emphasized that J_H stabilizes the gap at half filling, i.e., d^5 Mn, and reduces the gap for other fillings [38].

The role of Hund's coupling is highlighted in Fig. 3(b), which presents a DFT + DMFT calculation in the PM state that includes both $J_H = 0.9$ eV, along with a more realistic value of $U = 8$ eV [33]. The inclusion of J_H shifts the bands away from the Fermi level, opening a gap. PM LaMnPO has evolved, by including Hund's coupling, from a moderately correlated metal [$U = 10$ eV, $J_H = 0$: Fig. 3(a)] to a bona fide insulator [$U = 8$ eV, $J_H = 0.9$ eV: Fig. 3(b)].

Does the presence of AF order significantly affect the magnitude of the gap? Figure 3(c) presents a DFT + DMFT calculation of LaMnPO in the AF state for the same $U = 8$ eV, $J_H = 0.9$ eV (a similar calculation was previously reported but for $U = 6$ eV, $J_H = 0.9$ eV [5]). Energy cuts from Figs. 3(b) and 3(c) of the spectral function $A(k,\omega)$ at high symmetry points are presented in Fig. 3(d). The direct charge gaps, defined from the maxima of $A(k,\omega)$, are calculated to be rather insensitive to AF order and are in good agreement with the experimental values [Fig. 2(b)], showing that Δ is well accounted for when J_H is considered as well as U. The indirect gap is defined from the conduction band minimum at M to the valence band maximum at Γ [Fig. 3(d)]. While the indirect gap has decreased substantially from 0.74 ± 0.05 eV in the AF state to 0.4 ± 0.05 eV in the PM state, it is still much larger than the activation gap of 0.1 eV found in resistivity measurements [14], suggesting that the conduction in LaMnPO is still dominated by in-gap states in the PM phase.

We have presented a combined experimental and theoretical study of LaMnPO which shows that exchange coupling J plays a minimal role in determining the charge gap Δ. The argument rests on three observations. First, there is only a 10 % reduction in Δ between T_N and the mean-field temperature, where AF correlations vanish. Second, J sets the scale for the fraction of Δ that can vanish for $T \gg T_N$ and we fit the spin waves detected in inelastic neutron scattering measurements to the Heisenberg model to show that $J \ll \Delta$. Finally, electronic structure calculations show that Δ persists in the absence of AF order, prompting our identification of LaMnPO as a Mott-Hund's insulator.

Although LaMnPO shares the insulating AF ground state of the cuprates, its multiorbital nature and the strong Hund's coupling J_H associated with its half-filled Mn d shell establish that it is a more strongly correlated and thus insulating version of the metallic Fe-based pnictides. Substantial charge fluctuations are observed in LaMnPO relative to the d^5 (Mn^{2+}) state [5], and high pressures drive the transition to a metallic state, followed at higher pressures by the collapse of AF order [15]. This strong d^5 character, where J_H adds to the on-site Coulomb interaction U, is likely to dominate well into the metallic state, making LaMnPO substantially more correlated than isostructural LaFeAsO, where the effective interaction $U_{\text{eff}} = U - J_H$ [38]. So far, superconductivity is yet to be observed in pressurized LaMnPO or related Mn-pnictide compounds. While it may be tempting to ascribe this to overly strong electronic correlations, it is possible that LaMnPO, as the cuprates, requires doping as well as pressure to drive superconductivity. Often the highest superconducting transition temperatures require metallization accompanied by the collapse of AF order. Despite the multiorbital character associated with Hund's coupling, these conditions have been met in other Mott-Hund's insulators [39]. It is possible that the identification of a suitable dopant, perhaps combined with pressure, may yet cause these two instabilities to occur simultaneously in LaMnPO, opening the door to another family of unconventional superconductors.

We acknowledge the Office of the Assistant Secretary of Defense for Research and Engineering for providing the NSSEFF funds that supported this research. We acknowledge the support of the National Institute of Standards and Technology, US Department of Commerce in providing neutron research facilities used in this work. Research at the Spallation Neutron Source at Oak Ridge National Laboratory was sponsored by the Scientific User Facilities Division, Office of Basic Energy Sciences, US Department of Energy.

[1] M. Imada, A. Fujimori, and Y. Tokura, Rev. Mod. Phys. **70**, 1039 (1998).

[2] N. F. Mott, Proc. Phys. Soc., London, Sect. A **62**, 416 (1949).

[3] W. Bronger and P. Müller, J. Less Common Metals **100**, 241 (1984).

[4] A. Continenza, S. Picozzi, W. T. Geng, and A. J. Freeman, Phys. Rev. B **64**, 085204 (2001).

[5] J. W. Simonson, Z. P. Yin, M. Pezzoli, J. Guo, K. Post, A. Efimenko, N. Hollmann, Z. Hu, H.-J. Lin, C.-T. Chen, C. Marques, V. Leyva, G. Smith, J. W. Lynn, L. L. Sun, G. Kotliar, D. N. Basov, L. H. Tjeng, and M. C. Aronson, Proc. Natl. Acad. Sci. USA **109**, E1815 (2012).

[6] P. A. Lee, N. Nagaosa, and X. G. Wen, Rev. Mod. Phys. **78**, 17 (2006).

[7] D. C. Johnston, Adv. Phys. **59**, 803 (2010).

[8] Y. Kamihara, T. Watanabe, M. Hirano, and H. Hosono, J. Am. Chem. Soc. **130**, 3296 (2008).

[9] A. Pandey, R. S. Dhaka, J. Lamsal, Y. Lee, V. K. Anand, A. Kreyssig, T. W. Heitmann, R. J. McQueeney, A. I. Goldman, B. N. Harmon, A. Kaminski, and D. C. Johnston, Phys. Rev. Lett. **108**, 087005 (2012).

[10] B. Saparov and A. S. Sefat, J. Solid State Chem. **204**, 32 (2013).

[11] A. Georges, G. Kotliar, W. Krauth, and M. J. Rozenberg, Rev. Mod. Phys. **68**, 13 (1996).

[12] I. Lo Vecchio, A. Perucchi, P. Di Pietro, O. Limaj, U. Schade, Y. Sun, M. Arai, K. Yamaura, and S. Lupi, Sci. Rep. **3**, 2990 (2013).
[13] Z. P. Yin, K. Haule, and G. Kotliar, Nat. Mater. **10**, 932 (2011).
[14] J. W. Simonson, K. Post, C. Marques, G. Smith, O. Khatib, D. N. Basov, and M. C. Aronson, Phys. Rev. B **84**, 165129 (2011).
[15] J. Guo, J. W. Simonson, L. L. Sun, Q. Wu, P. Gao, C. Zhang, D. Gu, G. Kotliar, M. C. Aronson, and Z. Zhao, Sci. Rep. **3**, 2555 (2013).
[16] H. Yanagi, T. Watanabe, K. Kodama, S. Iikubo, S. Shamoto, T. Kamiya, M. Hirano, and H. Hosono, J. Appl. Phys. **105**, 093916 (2009).
[17] J. W. Lynn, Y. Chen, S. Chang, Y. Zhao, S. Chi, W. Ratcliff II, B. G. Ueland, and R. W. Erwin, J. Res. NIST **117**, 61 (2012).
[18] G. E. Granroth, A. I. Kolesniov, T. E. Sherline, J. P. Clancy, K. A. Ross, J. P. C. Ruff, B. D. Gaulin, and S. E. Nagler, J. Phys.: Conf. Ser. **251**, 012058 (2010).
[19] G. Kotliar, S. Y. Savrasov, K. Haule, V. S. Oudovenko, O. Parcollet, and C. A. Marianetti, Rev. Mod. Phys. **78**, 865 (2006).
[20] K. Haule, C. H. Yee, and K. Kim, Phys. Rev. B **81**, 195107 (2010).
[21] P. Blaha, K. Schwarz, G. Madsen, D. Kvasnicka, and J. Luitz, WIEN2K package, http://www.wien2k.at.
[22] J. P. Perdew, K. Burke, and M. Ernzerhof, Phys. Rev. Lett. **77**, 3865 (1996).
[23] A. T. Nientiedt, W. Jeitschko, P. G. Pollmeier, and M. Brylak, Z. Naturforsch. B: J. Chem. Sci. **52**, 560 (1997).
[24] A. Zheludev, RESLIB, Oak Ridge National Laboratory, 2001.
[25] S. Chakravarty, B. I. Halperin and D. R. Nelson, Phys. Rev. B **39**, 2344 (1989).
[26] D. C. Johnston, in *Handbook of Magnetic Materials*, edited by K. H. J. Buschow (Elsevier, Amsterdam, 1997), Vol. 10, Chap. 1, pp. 1–237.
[27] M. Takahashi, Phys. Rev. B **40**, 2494 (1989).
[28] P. J. Brown, in *International Tables for Crystallography*, 1st ed., edited by A. J. C. Wilson (Kluwer Academic, Dordrecht, 1992), Vol. C, Chap. 4.4.5, pp. 391–399.
[29] I. A. Zaliznyak, in *Handbook of Magnetism and Advanced Magnetic Materials*, edited by H. Kronmüller and S. Parkin (Wiley, Hoboken, NJ, 2007).
[30] D. C. Johnston, R. J. McQueeney, B. Lake, A. Honecker, M. E. Zhitomirsky, R. Nath, Y. Furukawa, V. P. Antropov, and Y. Singh, Phys. Rev. B **84**, 094445 (2011).
[31] E. Rosencher and B. Vinter, *Optoelectronics* (Cambridge University Press, Cambridge, UK, 2002).
[32] G. Kotliar and D. Vollhardt, Phys. Today **57**(3), 53 (2004).
[33] A. Kutepov, K. Haule, S. Y. Savrasov, and G. Kotliar, Phys. Rev. B **82**, 045105 (2010).
[34] Z. P. Yin, K. Haule, and G. Kotliar, Nat. Phys. **7**, 294 (2011).
[35] K. Haule and G. Kotliar, New J. Phys. **11**, 025021 (2009).
[36] J. Mravlje, M. Aichhorn, T. Miyake, K. Haule, G. Kotliar, and A. Georges, Phys. Rev. Lett. **106**, 096401 (2011).
[37] Z. P. Yin, K. Haule, and G. Kotliar, Phys. Rev. B **86**, 195141 (2012).
[38] A. Georges, L. de' Medici, and J. Mravlje, Annu. Rev. Condens. Matter Phys. **4**, 139 (2013).
[39] J. Kunes, A. V. Yukoyanov, V. I. Anisimov, R. T. Scalettar, and W. E. Pickett, Nat. Mater. **7**, 198 (2008).